A visible light-responsive iodine-doped titanium dioxide nanosphere

Zhiqiao He[1], Liyong Zhan[1], Fangyue Hong[1], Shuang Song[1,*],
Zhengying Lin[2], Jianmeng Chen[1], Mantong Jin[1]

1. College of Biological and Environmental Engineering, Zhejiang University of Technology, Hangzhou 310032, China. E-mail: zqhe@zjut.edu.cn
2. Department of Chemical Engineering, Hangzhou Vocational & Technical College, Hangzhou 310018, China

Abstract

I-doped titanium dioxide nanospheres (I-TNSs) were synthesized via a two-step hydrothermal synthesis route, their potential for the efficient utilization of visible light was evaluated. The prepared anatase-phase I-TNSs had a bimodal porous size distribution with a Brunauer-Emmett-Teller surface area of 76 m^2/g, a crystallite size of approximately 14 nm calculated from X-ray diffraction data, and a remarkable absorption in the visible light region at wavelengths > 400 nm. The photocatalytic activity of the samples was evaluated by decoloration of Methyl Orange in aqueous solution under visible light irradiation in comparison to the iodine-doped TiO_2 (I-TiO_2). The I-TNSs showed higher photocatalytic efficiency compared with I-TiO_2 after irradiation for 180 min even though the latter had a much greater surface area (115 m^2/g). It was concluded that the surface area was not the predominant factor determining photocatalytic activity, and that the good crystallization and bimodal porous nanosphere structure were favourable for photocatalysis.

Key words: I-doped titanium dioxide; nanospheres; Methyl Orange; visible light

DOI: 10.1016/S1001-0742(10)60389-0

Citation: He Z Q, Zhan L Y, Hong F Y, Song S, Lin Z Y, Chen J M et al., 2011. A visible light-responsive iodine-doped titanium dioxide nanosphere. *Journal of Environmental Sciences*, 23(1): 166–170.

Introduction

The use of iodine-doped TiO_2 (I-TiO_2) to conserve solar energy efficiently has initiated a new area of research. Earlier studies focused mainly on the effects of iodine on the physical-chemical properties of the photocatalyst and its performance in photocatalysis. The contribution of iodine to band gap narrowing has been evaluated (Hong et al., 2005; Long et al. 2006; He et al., 2008; Song et al., 2008; Su et al., 2008; Tojo et al., 2008; Liu et al., 2009). By first principle calculations, some researchers suggested that the I 5p and/or I 5s orbitals mixing with O2p in the valence band and Ti 3d orbitals in the conduction bands was responsible for the response to visible light (Long et al. 2006; Tojo et al., 2008). Some asserted that two atomic configurations, I-O-I and I-O-Ti, coexisted on the surface of I-TiO_2 and contributed to the extension of light absorption in the visible region (Su et al., 2008; Liu et al., 2009). Extensive investigations have been devoted to co-doping TiO_2 with iodine and other elements in attempts to further increase the photocatalytic activity. For example, TiO_2 photocatalysts co-doped with iodine and rare earths cerium or lanthanum showed significantly higher photocatalytic activity in the degradation of oxalic acid (He et al., 2008; Song et al., 2008). However, those

studies did not investigate iodine-doped TiO_2 nanospheres (I-TNSs) as potential photocatalysts.

The morphology and microstructure of titanium dioxide (titania) play a crucial role in the photocatalytic process (Liu et al., 2003, 2008). There have been attempts to synthesize TiO_2 with various nanostructures, including nanotubes (Mor et al., 2006), nanorods (Feng et al., 2005), nanowires (Miao et al., 2002) and nanospheres (Yang et al., 2004; Li et al., 2007). The nanospheres have the advantages of a low density, a large surface area and good stability and optical scattering properties (Dong et al., 2009). In the present study, we prepared and characterized the I-doped titanium dioxide nanospheres (I-TNSs) via a two-step hydrothermal method, and the photocatalytic activity was estimated in terms of the decoloration of Methyl Orange (MO) under visible light irradiation.

1 Materials and methods

1.1 Preparation and characterization of the photocatalyst

Herein, the I-TNSs were prepared via a two-step hydrothermal synthesis route using Ti(SO$_4$)$_2$ as the precursor. Typically, a total of 3.6 g of Ti(SO$_4$)$_2$ was dissolved in 40 mL of distilled water and 15 g of glucose in 80 mL of water was added immediately to give a molar ratio of glucose/Ti

of 5:1. The mixture was transferred to a Teflon-lined stainless steel autoclave (178 mL capacity), and heated in an oven at 180°C for 24 hr. The autoclave was removed from the oven and allowed to cool to room temperature. The precipitate was collected by centrifugation, washed several times with distilled water and then with absolute alcohol. After drying in vacuo at 60°C for 5 hr, the product was calcined in a muffle furnace at 450°C for 4 hr at a heating rate of 4°C/min to form the TiO_2 nanospheres. The second step of the hydrothermal process was to heat 0.5 g of TiO_2 nanospheres with 160 mL of iodic acid in the autoclave at 150°C for 24 hr. The white precipitate was collected and air-dried overnight at 80°C, followed by calcination at 400°C for 2 hr. For comparison, I-TiO_2 nanoparticles were synthesized as described in literature (Hong et al., 2005).

1.2 Photocatalytic activity measurement

The photocatalytic experiment was conducted in a cylindrical Pyrex glass reactor (diameter 16 cm; height 20 cm; total capacity 3 L) containing 1.5 L of 10 mg/L MO aqueous solution and 1.5 g of the photocatalyst stirred continuously with a magnetic follower. The reaction aqueous solution was irradiated with a 500 W dysprosium lamp (Beijing Electric Light Sources Research Institute, China), which has a spectrum very close to solar light, through 1 L of 2 mol/L sodium nitrite as a filter for visible light ($\lambda > 400$ nm). A similar method was used by Maeda et al. (2009). The detailed procedure was described earlier (He et al., 2008). The absorbance of the MO reaction solution was determined with a UV-Visible spectrophotometer (T6, Beijing Purkinje General Instrument Co., Ltd., China).
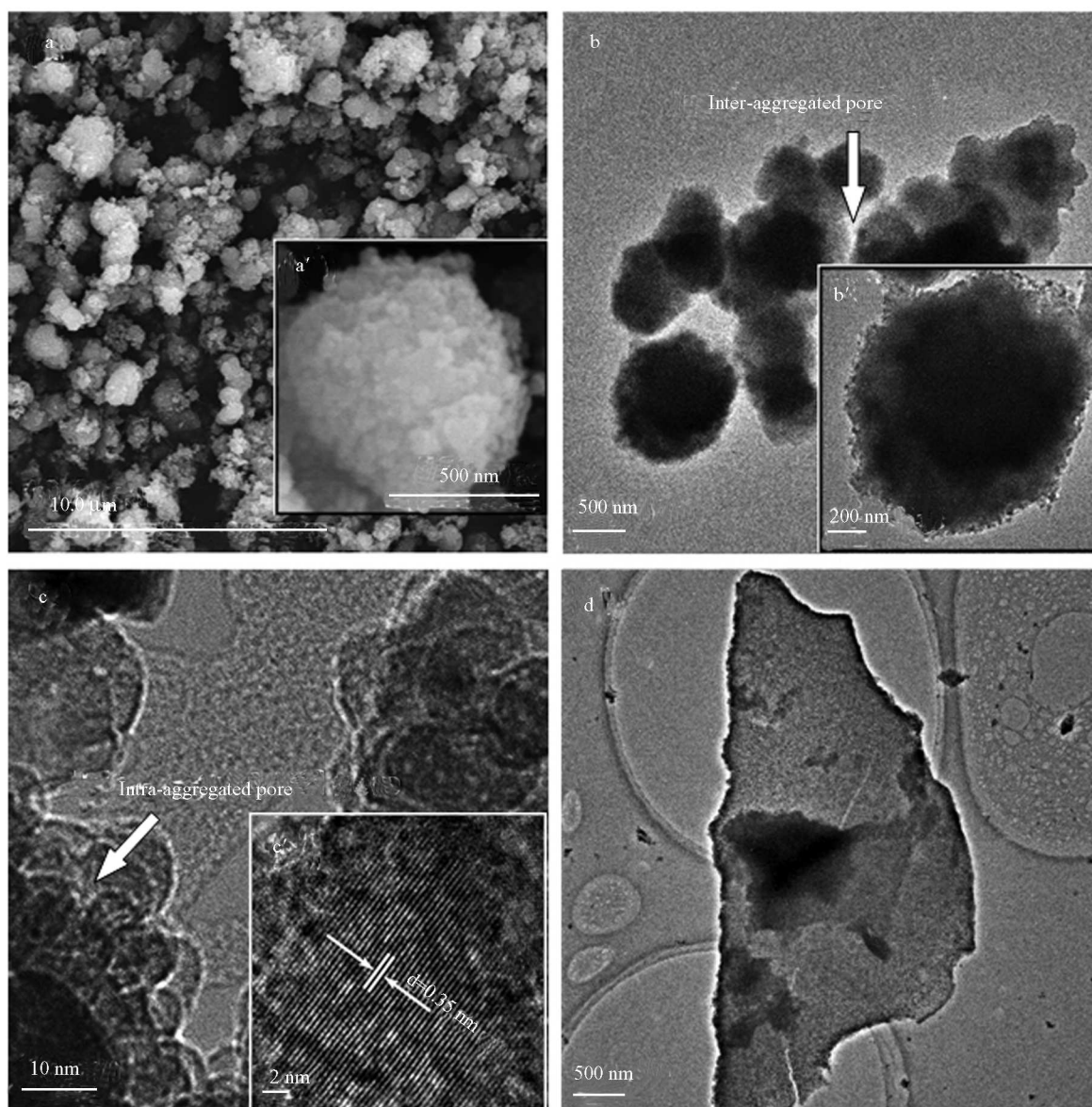

Fig. 1 Morphological images of the I-TNSs and I-TiO_2. (a) SEM image of the I-TNSs, inset was the magnified image; (b) TEM micrograph of the I-TNSs, inset was a magnified TEM image; (c) high resolution (HR)-TEM images of the I-TNSs, the sample exhibited the d-spacing value of 0.35 nm; (d) TEM micrograph of the I-TiO_2.

2 Results and discussion

2.1 Catalyst characterization

The morphology of I-TNSs examined by scanning electron microscopy (SEM) is shown in Fig. 1a. The nanospheres, although not perfectly spherical, had an average diameter of 300–500 nm and appeared to have a rough surface morphology. Further identification of the configuration of spherical nanostructures was achieved by transmission electron microscopy (TEM). Figs. 1b and b′ show that the diameters of I-TNSs are in accordance with the SEM measurements and the nanospheres are not hollow. In addition, extra-large textural meso- and macro-pores (interaggregated pores) formed by interaggregated spherical particles are evident in Fig. 1b. The spherical architecture was formed by close aggregation of prima-ry crystallites with a size of 14 nm, resulting in large quantities of narrow interstitial pores (intra-aggregated pores) on the verge of nanospheres (Fig. 1c). The lattice fringe of the small crystallites was 0.35 nm, as shown in Fig. 1d, corresponding to the lattice spacing of the (101) crystallographic plane of anatase TiO_2, indicating good crystallization of anatase I-TNSs. For comparison, TEM was used to observe the surface and inner structure of I-TiO_2 under the same magnification (Fig. 1d). It is obvious from the mass contrast that the dense particle included well-dispersed I-TiO_2 particles. Nonetheless, no obvious nanospheres consisting of I-TiO_2 crystallites could be observed.

The X-ray diffraction (XRD) patterns of I-TNSs and I-TiO_2 are shown in Fig. 2a. Both patterns exhibit char-acteristic diffraction peaks at 2θ values of 25.3°, 37.8°, 48.0°, 53.9°, 62.7°, 70.2° and 75.0°, matching the (101), (004), (200), (211), (204), (220) and (215) planes of anatase titania (JCPDS Card no. 21-1272), without any additional diffraction peak. In comparison to I-TiO_2, the intensities of characteristic diffraction peaks of I-TNSs increased sharply, implying that well crystallized I-TNSs have been synthesized under the two-step hydrothermal synthesis route. Furthermore, the average crystal size of I-TNSs was calculated to be approximately 14 nm from the width at half-height of the diffraction peak at 2θ value of 25.3° based on the Debye-Scherrer equation, which is in good agreement with the TEM results, as shown in Fig. 1c.

The UV-Visible diffuse reflectance spectra were ob-tained to confirm the optical properties of I-TNSs and I-TiO_2 catalysts, and the results are shown in Fig. 2b. It is well known that pure TiO_2 only has an absorption band in the UV region, whereas the absorbance of both I-TNSs and I-TiO_2 extends from the UV to the visible region, and I-TiO_2 shows a greater red shift than I-TNSs. The onset wavelength (λ) for I-TNSs and I-TiO_2 is located at 402 nm and 470 nm, respectively, which is consistent with the buff colour of the samples. The band gap (E_g) was calculated as 3.08 and 2.64 eV, based on Eq. (1) (Wei et al., 2007):
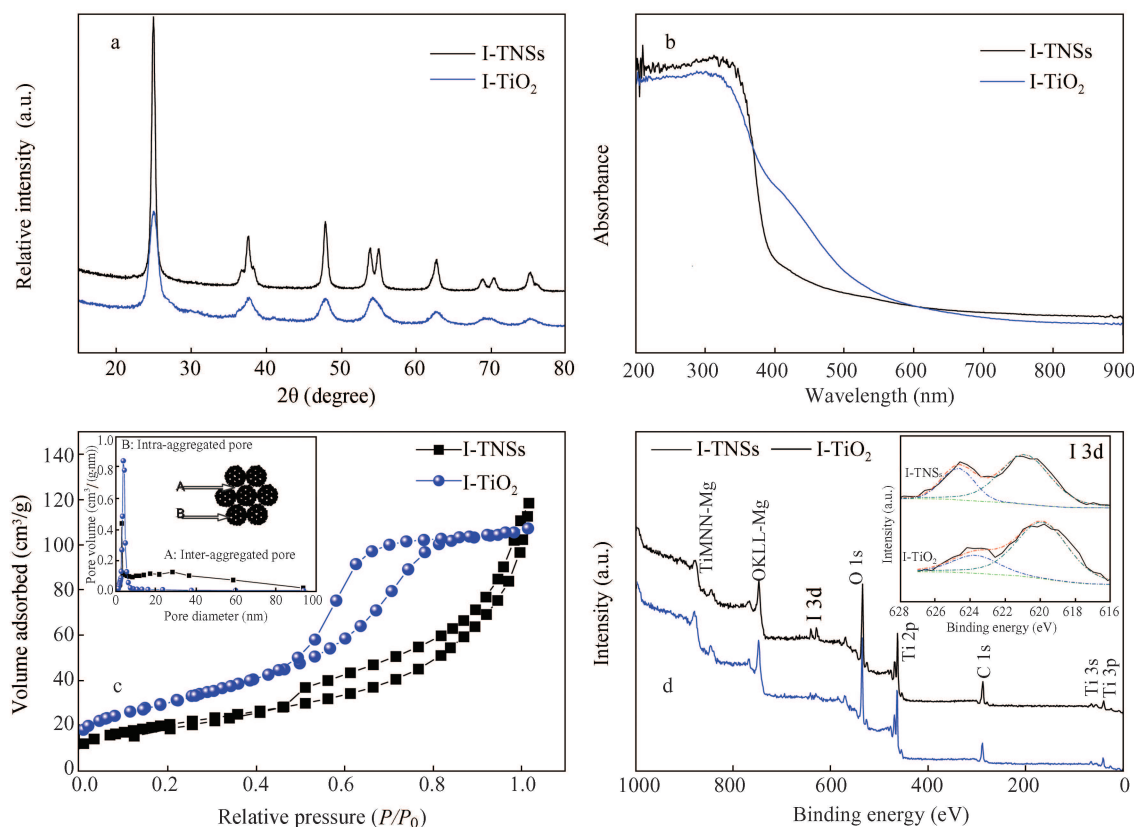
$$E_g = 1239.8/\lambda \qquad (1)$$

Fig. 2 (a) XRD patterns of I-TNSs and I-TiO_2; (b) UV-vis diffuse-reflectance spectra of I-TNSs and I-TiO_2; (c) N_2 low-temperature adsorption-desorption isotherms, inset was desorption BJH pore size distribution plots; (d) XPS spectra of I-TNSs and I-TiO_2, inset was the region scan of I 3d.

Figure 2c shows the N_2 adsorption-desorption isotherms of I-TNSs and I-TiO$_2$ photocatalysts, as well as the corresponding pore size distribution plot determined from the adsorption branch by the Barrett-Joyner-Halenda (BJH) method. The isotherm for I-TiO$_2$ exhibits a typical IV-like isotherm with an H2 hysteresis loop, and the average pore diameter is 4.1 nm. The isotherm of I-TNSs shows two distinct capillary condensation steps at relative pressure (P/P_0) of 0.12–0.45 and 0.45–1, suggesting the simultaneous presence of smaller and larger pores with sizes of 3.0 nm and 30 nm. This is consistent with the bimodal pore-size distribution of I-TNSs (Fig. 2c, inset). A bimodal pore-size distribution is ascribed to two types of aggregates in the catalysts: the smaller pores (intra-aggregated pores) are located between intra-agglomerated primary particles, whereas the larger pores (inter-aggregated pores) are assigned to the inter-aggregated secondary particles, as observed by TEM. Besides, the Brunauer-Emmett-Teller (BET) surface areas of I-TNSs and I-TiO$_2$ catalysts were 76 m^2/g and 115 m^2/g, respectively. The relatively low BET surface area for I-TNSs might be the reason that the two calcination processes occurred during preparation of the catalyst. Similar outcomes have been reported by Fei et al. (2007).

X-ray photoelectron spectroscopy (XPS) analysis was used to investigate the composition and valence states of the elements in I-TNSs and I-TiO$_2$. The survey spectra reveal mainly the characteristic signal of I 3d, Ti 2p, O 1s and C 1s (Fig. 2d). From the high-resolution XPS spectra of the I 3d region of both samples (Fig. 2d, inset), we can see obviously doublet peaks at banding energies (BE) of 624.5 eV (I 3d$_{5/2}$) and 620.5 eV (I 3d$_{3/2}$), respectively, implying that multiple valence forms of iodine existed in the samples. The BE of I 3d$_{5/2}$ was higher than that of I 3d$_{5/2}$ in HIO$_3$ (623 eV). High BE is attributed to a high valence state because decreasing the density of outer electrons will lead to increasing BE. We concluded that heptavalent (I^{7+}) and negatively charged (I$^-$) iodine species were generated via a disproportionation reaction of the iodate ion during the hydrothermal process. Namely, the BE of I 3d$_{5/2}$ is assigned to I^{7+}, which has been shown to exist in the form of periodate (IO$_4^-$) (Liu et al., 2009), and the BE of I 3d$_{3/2}$ is assigned to I$^-$. The ionic radius of I$^-$ (0.216 nm) and that of the IO$_4^-$ group are much larger than those of Ti^{4+} (0.068 nm) and O$_2^-$ (0.124 nm) (Liu et al., 2006; Su et al., 2008), it is theoretically impossible for iodine to be incorporated into the TiO$_2$ lattice and substitute Ti^{4+} or O^{2-} with respect to radius matching (Su et al., 2008). Thus, I$^-$ and IO$_4^-$ should diffuse to the surface of I-TNSs and I-TiO$_2$, coexisting in the form of IO$_4^-$/I$^-$ species as described by Su et al. (2008) and Liu et al., 2009).

2.2 Photocatalytic activity

The photocatalytic activity of synthesized I-TNSs and I-TiO$_2$ catalysts was studied for decoloration of MO under visible light irradiation (Fig. 3). As a comparison, direct photolysis of MO without a catalyst was done under analogous conditions. No obvious decoloration of MO was
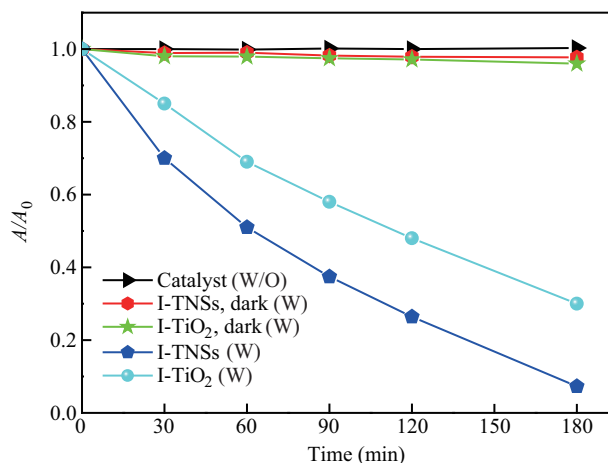

Fig. 3 Decoloration of MO in aqueous solution with different photocatalyst (I-TNSs, and I-TiO$_2$) under visible light irradiation. The reference experiments (without catalyst, with I-TNSs in the dark condition, with I-TiO$_2$ in the dark condition) are suggested for clarifying the decoloration.

observed in the absence of catalysts, suggesting that direct photolysis of MO was negligible under our experimental conditions. In addition, the adsorption of MO in darkness after 180 min were 3.8% and 2.3% for I-TiO$_2$ and I-TNSs, respectively, indicating that adsorption did not contribute significantly to the decoloration of MO. According to Fig. 3, the decoloration efficiency of 92.8% was acquired from the I-TNSs catalyst after reaction for 180 min, which is 23% higher than that from I-TiO$_2$, although the I-TiO$_2$ has a relatively high adsorption capacity. Generally, a large surface area is favourable for a high level of photocatalytic activity, as a larger surface area provides more active sites and, thus, more photocatalytic reaction centres. Nevertheless, the photocatalytic process did not follow this trend in this study. I-TiO$_2$ had a larger surface area (115 m^2/g) than that of I-TNSs (76 m^2/g), but the efficiency of photocatalysis was not increased concomitantly. Therefore, we conclude that the surface area is not the only factor controlling photocatalytic activity. Similar results have been reported by other researchers (Wang et al., 2009). The problem was how to best elucidate the superior photocatalytic performance of I-TNSs?

On the basis of the results of XRD studies, the improvement of photocatalytic activity can be ascribed to the enhancement of anatase crystallization compared with that of I-TiO$_2$, because good crystallization is beneficial to retarding the recombination of photogenerated electron-holes by decreasing the number of defects (Yu et al., 2007). Theoretically, the degree of crystallization of I-TiO$_2$ can increase with the annealing temperature. However, previous studies have proved that high-temperature annealing at > 400°C generates the rutile phase of I-TiO$_2$, thus inhibiting photocatalytic activity (Hong et al., 2005). Therefore, under the same calcination conditions, better crystallization of I-TNSs should be one of the reasons responsible for the enhanced decoloration of MO. A similar outcome has been described by Yu et al. (2007).

In addition, intra-aggregated pores in the bimodal pores of the nanosphere structure facilitate reactant and product access to the reactive sites on the photocatalyst

surface. Interaggregated pores favour the enhancement of photocatalytic activity via increasing light-harvesting efficiency by multiple scattering within the porous framework and providing more efficient transport channels for the reactant molecules to approach the reactive sites on the framework walls of the small mesopores. The explanation has been explicitly demonstrated by many researchers (Zhang and Yu, 2003; Liu et al., 2006).

3 Conclusions

In summary, we have developed a method for the preparation of I-TNSs with an anatase framework. The improved photocatalytic activity of I-TNSs towards the decoloration of MO under visible light irradiation is strongly dependent on good crystallization and the bimodal porous structure of the nanospheres. The materials described here may be helpful in new efforts for the preparation and characterization of excellent visible light response TiO_2 photocatalysts.

Acknowledgments

References

Dong X, Tao J, Li Y Y, Zhu H, 2009. Enhanced photoelectrochemical properties of F-containing TiO_2 sphere thin film induced by its novel hierarchical structure. *Applied Surface Science*, 255(16): 7183–7187.

Fei H L, Liu Y P, Li Y P, Sun P C, Yuan Z Y, Li B H et al., 2007. Selective synthesis of borated meso-macroporous and mesoporous spherical TiO_2 with high photocatalytic activity. *Microporous and Mesoporous Materials*, 102(1/2/3): 318–324.

He Z Q, Xu X, Song S, Xie L, Tu J J, Chen J M et al., 2008. A visible light-driven titanium dioxide photocatalyst codoped with lanthanum and iodine: an application in the degradation of oxalic acid. *Journal of Physical Chemistry C*, 112(42): 16431–16437.

Hong X T, Wang Z P, Cai W M, Lu F, Zhang J, Yang Y Z et al., 2005. Visible-light-activated nanoparticle photocatalyst of iodine-doped titanium dioxide. *Chemistry of Materials*, 17(6): 1548–1552.

Liu G, Sun C H, Yan X X, Cheng L N, Chen Z G, Wang X W

et al., 2009. Iodine doped anatase TiO_2 photocatalyst with ultra-long visible light response: correlation between geometric/electronic structures and mechanisms. *Journal of Materials Chemistry*, 19(18): 2822–2829.

Liu G, Chen Z G, Dong C L, Zhao Y N, Li F, Lu G Q et al., 2006. Visible light photocatalyst: iodine-doped mesoporous titania with a bicrystalline framework. *Journal of Physical Chemistry B*, 110(42): 20823–20828.

Liu H L, Zhou D, Li X Z, Yue P T, 2003. Photoelectrocatalytic degradation of rose bengal. *Journal of Environmental Sciences*, 15(5): 595–599.

Liu L, Liu H J, Zhao Y P, Wang Y Q, Duan Y Q, Gao G D et al., 2008. Directed synthesis of hierarchical nanostructured TiO_2 catalysts and their morphology-dependent photocatalysis for phenol degradation. *Environmental Science and Technology*, 42(7): 2342–2348.

Long M C, Cai W M, Wang Z P, Liu G Z, 2006. Correlation of electronic structures and crystal structures with photocatalytic properties of undoped, N-doped and I-doped TiO_2. *Chemical Physics Letters*, 420(1/2/3): 71–76.

Maeda K, Masuda H, Domen K, 2009. Effect of electrolyte addition on activity of $(Ga_{1-x}Zn_x)(N_{1-x}O_x)$ photocatalyst for overall water splitting under visible light. *Catalysis Today*, 147(3/4): 173–178.

Song S, Tu J J, Xu L J, Xu X, He Z Q, Qiu J P et al., 2008. Preparation of a titanium dioxide photocatalyst codoped with cerium and iodine and its performance in the degradation of oxalic acid. *Chemosphere*, 73(9): 1401–1406.

Su W Y, Zhang Y F, Li Z H, Wu L, Wang X X, Li J Q et al., 2008. Multivalency iodine doped TiO_2: preparation, characterization, theoretical studies, and visible-light photocatalysis. *Langmuir*, 24(7): 3422–3428.

Tojo S, Tachikawa T, Fujitsuka M, Majima J, 2008. Iodine-doped TiO_2 photocatalysts: correlation between band structure and mechanism. *Journal of Physical Chemistry C*, 112(38): 14948–14954.

Wang J, Li M, Zhi M J, Manivannan A, Wu N Q, 2009. Hydrothermal synthesis and photocatalytic activity of titanium dioxide nanotubes, nanowires and nanospheres. *Fractal Geometry and Stochastics IV*, 61: 71–76.

Wei C H, Tang X H, Liang J R, Tan S Y, 2007. Preparation, characterization and photocatalytic activities of boron and cerium-codoped TiO_2. *Journal of Environmental Sciences*, 19(1): 90–96.

Yu J G, Zhang L J, Cheng B, Su Y R, 2007. Hydrothermal preparation and photocatalytic activity of hierarchically sponge-like macro-/mesoporous titania. *Journal of Physical Chemistry C*, 111(28): 10582–10589.

Zhang L Z, Yu J C, 2003. A sonochemical approach to hierarchical porous titania spheres with enhanced photocatalytic activity. *Chemical Communications*, (16): 2078–2079.